"This is the peer reviewed version of the following article: Bin Cai, Dan Wen, Wei Liu, Anne-Kristin Herrmann, Albrecht Benad and Alexander Eychmüller (2015). Function-led Design of Aerogels: Self-assembly of Alloyed PdNi Hollow Nanospheres for Efficient Electrocatalysis. Angewandte Chemie-international Edition, 2015, Vol. 54(44), pp. 13101--13105, which has been published in final form at DOI: 10.1002/anie.201505307.
This article may be used for non-commercial purposes in accordance with Wiley Terms and Conditions for Self-Archiving."

Function-led Design of Aerogels: Self-assembly of Alloyed PdNi Hollow Nanospheres for Efficient Electrocatalysis

Bin Cai, Dan Wen, Wei Liu, Anne-Kristin Herrmann, Albrecht Benad and Alexander Eychmüller*

Physical Chemistry, TU Dresden

Bergstrasse 66b, 01062 Dresden (Germany)

E-mail: alexander.eychmueller@chemie.tu-dresden.de

Homepage: http://www.chm.tu-dresden.de/pc2/

Abstract: Amelioration of the building blocks is a plausible approach to graft aerogels with distinguished properties while preserving the aerogel superiority. However, the incorporation of designated properties into metallic aerogels, especially catalytically beneficial morphologies and transition metal doping, still remains a challenge. Here, we report on the first case of an aerogel electrocatalyst composed entirely of alloyed PdNi hollow nanospheres (HNSs) with controllable chemical composition and shell thickness. The synergy of the transition metal doping, combined with the hollow building blocks and the three dimensional network structure make the PdNi HNS aerogels promising electrocatalysts towards ethanol oxidation, among which the $Pd_{83}Ni_{17}$ HNS aerogel shows a 5.6-fold enhanced mass activity compared to commercial Pd/C. This work expands the exploitation approach of electrocatalytic properties of aerogels into morphology and composition control of its building blocks.

Assemblies of nanomaterials into macroscopic aerogel frameworks have currently attracted great interest in the nanotechnology revolution due to their extremely high porosity and large specific surface area.[1] Since the pioneering work on aerogels from the early 1930s, different inorganic or organic building blocks have been employed to explore their potential applications.[2] For instance, Leventis et al. led the research to metallic aerogels (non-noble metals, including Fe, Co, Cu, etc.) by a carbothermal method.[3] Brock et al. made exceptional contributions to the development of semiconductor and quantum dots derived aerogels.[4] Arachchige et al. expanded Ag-based metallic aerogels into controlled morphologies.[5] Meanwhile, our group has reported a series of pure and mixed aerogels (made of noble metal, semiconductor and quantum dots).[6] The aerogels reported up to now have

shown great application potential in the area of catalysis, energy storage, thermoresistors, etc.[7] However, the application studies of these aerogels lags far behind their preparation prosperity, especially the metal-involving aerogels.[8]

Metallic aerogels combine the advantages of metals and aerogels, such as the metallic backbone (enable fast electron-transfer kinetics), large surface area (supply more reactive sites), high porosity (accelerate mass transfer) and self-supportability (eliminate support corrosion), which unleashed tremendous potential in electrocatalysis.[9] Nonetheless, the investigation of metallic aerogel electrocatalysts is still in the early stage and is largely limited by the solid building blocks.[7] The previous reports have shown that the intimate relationship between the nano-component and the macro-aerogel provides a straightforward modality for the deliberate tailoring of aerogel properties by amelioration of the building blocks. Thus, it is of great interest to inject new properties into aerogel catalysts *via* the expectant optimization of the nano building blocks. From a noble metal electrocatalyst perspective, regulation of the morphology and alloying with transition metals remain the most efficient ways to meet the industrial requirements.[10] Despite the recent reports of electrocatalytic and bio-electrocatalytic activities upon pure Pd and PdPt metallic aerogels,[9] design of efficient aerogel electrocatalysts based on catalytically beneficial morphologies and transition metal doping has not been reported to date.

In this context, bimetallic aerogels which are composed entirely of alloyed PdNi hollow nanospheres (HNSs) were accomplished via a facile bottom-up method. The PdNi HNS building blocks connect and fuse into a well-defined three dimensional (3D) necklace-like network structure during the gelation process. It has been demonstrated that nanocrystals with hollow interior exhibit superior catalytic activities than their solid counterparts and nickel represents an ideal transition metal to manipulate the electronic properties to achieve the greatest potential of the noble metal.[11] The inheritance of the excellent genes from the hollow structure, the Pd-Ni alloy and the aerogel architectures impart high electrocatalytic activity to the as-prepared PdNi HNS aerogel. As shown in Scheme 1, the alloyed PdNi HNSs, as the building blocks with a diameter of ca. 30 nm and shell thickness of ca. 5 nm, were synthesized via a galvanic replacement method using Ni nanoparticles (NPs) as sacrificial templates (Figure S1). Since the aqueous solutions of the HNSs are normally very stable in the as-prepared state, it is necessary to concentrate the sols and eliminate parts of the stabilizers to reach a “metastable state” (the highly concentrated sols are still very stable after 2 months).[6a] The gelation process was achieved by heating the concentrated sols at 348 K for 6 hours. After the solvent of the resulting hydrogels was exchanged with acetone, self-supported monolithic HNS aerogels were obtained after the evaporation of the pore liquid using supercritical drying (Figure S2).

As shown in the scanning electron microscopy (SEM) and transmission electron microscopy (TEM) images (Figure 1a-c and S3), the PdNi HNS aerogel has an excellent 3D porous network structure which is formed from fusion and random interconnection of individual HNSs. The necklace-like backbone exhibits similar diameter (~30 nm) as its HNS building blocks, indicating the HNSs remain intact during the gelation and drying processes. The crystalline properties of the HNSs and their fused junction area were demonstrated by high resolution TEM (HR-TEM) images (Figure 1d and S4). The regular face-centered-cubic (fcc) lattice is observed throughout the “necklace” region. Lattice spacings of about 2.30 Å which can be indexed to the (111) planes are widely distributed at all locations. The crystalline

properties are further examined by X-ray diffraction (XRD) (Figure 2f), which shows that all the four characteristic peaks of the PdNi alloy are shifted towards larger diffraction angles, suggesting a lattice contraction with increasing Ni content.[12] The slight shrinkage of the lattice parameters compared with our previous pure Pd aerogel can be attributed to the permeation of Ni atoms into the Pd lattice which results in smaller crystallographic unit cells.[6b, 13] Figure 1e and f show the STEM energy-dispersive X-ray (STEM-EDX) line-scanning profiling and elemental mapping analysis, respectively. As is shown, Pd and Ni are both distributed throughout the HNSs and the signals in the shell area are stronger than in the core area, which reflect the formation of PdNi alloy and the hollow structure. X-ray photoelectron spectroscopy (XPS) was further employed to investigate the electronic environment of Pd and Ni in the HNS aerogel structure (Figure S5). Summarizing the EDX, XPS and ICP-OES analysis (cf. the Supporting Information), the Pd/Ni mole ratio of the alloyed HNS aerogel is 83:17, being denoted it as Pd83Ni17 HNS aerogel.

The physicochemical properties, including the electrocatalytic activities, of bimetallic nanoarchitectures are known to be highly dependent on the elemental composition.[14] Thus we added different amounts of Pd precursors in order to tune the composition of the resulting PdNi HNS aerogels. The Ni content of the HNS aerogels varies from 3 to 19 %, as the molar ratio of Ni/Pd precursors varies from 1:2 to 4:1 (Figure S6). The TEM images in Figure 2 present the increasing shell thickness and the decreasing diameters with the decrease of the Ni/Pd ratio. When the Ni/Pd ratio decreases to 1:2, the thickness of their shells and the diameter are reduced to ca. 7 and 23 nm, respectively, with a shrunken hollow interior and a more fused network structure. Conversely, more broken HNSs and small shell pieces are observed in the aerogel structure when the Ni/Pd ratio reaches 4:1. Thus, the Ni/Pd ratio of 3:1 (Pd83Ni17) is most suitable for realizing the thinnest shell while keeping the structure intact. The XRD analysis (Figure 2f) demonstrates that the PdxNiy HNS aerogels share the same fcc crystalline structure regardless of the compositional change. The more asymmetric diffraction peaks with increased of Ni content implies the incorporation of Ni atoms into the Pd lattice.[15]

Taking the Pd83Ni17 HNS aerogel as an example, the surface area and porosity were further evaluated from N2 physisorption isotherms (Figure S7). The adsorption isotherm combines the characteristics of type II and type IV which indicates the wide spread of both meso- and macro-pores within the aerogel structure. As estimated from a Brunauer-Emmett-Teller (BET) plot the surface area is 95.4 m2 g-1 which is in the range of that of noble metal nanoparticle-based aerogels (32-168 m2 g-1).[7] The pore size distribution analysis exhibits a distinct pore distribution peak at ~22 nm which is attributed to the hollow cavity of the building blocks. The density of the Pd83Ni17 HNS aerogel is estimated to 0.035 g cm-3 which further demonstrated the high porosity.

It is reasonable to anticipate that the HNS aerogels are electrochemically more accessible due to the combination of their hollow structure and the 3D network assembly. As shown in Figure 3a and S8, cyclic voltammograms (CVs) of PdxNiy HNS aerogels and Pd/C modified electrodes were obtained in 1 M NaOH solution. Their electrochemical active surface area (ECSA) values were estimated by employing the reduction charge of Pd oxide and assuming a charge density of 430 μC cm-2 for the formation of a PdO monolayer.[16] The PdxNiy HNS aerogels exhibit different ECSA values (56.9, 55.5, 54.7, 51.1 and 47.8 m2 g-1 with the Ni content varying from 19% to 3%), while the ECSA value of Pd/C is 42.3 m2 g-1.

Even more convincingly, the ECSA value of the Pd83Ni17 HNS building blocks is 45.2 m2 g-1, 1.23 times lower than their aerogel counterparts, indicating the significance of the aerogel structure in the preservation of ECSA. The higher ECSA values guarantee more active sites accessible, suggesting an increase in the utilization efficiency of Pd.[17] As summarized in Figure 3b, the mass activities (MAs) and specific activities (SAs) of the PdNi HNS aerogels are much higher than that of commercial Pd/C, among which the Pd83Ni17 HNS aerogel shows the highest MA (3.63 A mg-1) and SA (6.54 mA cm-2), 5.6 and 4.2 times higher than that of Pd/C (MA: 0.65 A mg-1, SA: 1.54 mA cm-2), respectively. In addition, the more negative onset potential (Figure S8) of the PdNi HNS aerogels compared to that of Pd/C indicates an enhancement in the kinetics of the ethanol oxidation reaction, which represents another crucial parameter to optimize an electrocatalyst. To further demonstrate the importance of the 3D network, we compared the MAs and SAs between the aerogel and its building blocks in the case of Pd83Ni17 (Figure 3c and S9). The MA is improved by 1.5 times upon the 3D network architecture, while the SAs do not show much difference due to their equal chemical properties.

The varying activities of the PdxNiy HNS aerogels are referable to both the morphology changes and the Ni content. To exclude the morphology interference and investigate the effect of the Ni content, we removed most of the Ni from the Pd83Ni17 HNSs by HCl etching and obtaining by this the Pd96Ni4 HNS aerogel which is labelled as Pd96Ni4-HCl (Figure S10). Most of the ECSA survived the HCl etching, indicating the robustness of the HNS aerogel structure (Figure S11a). However, 28.4% of the MA and 24.4% of the SA are lost in comparison to the Ni-rich HNS aerogels (Figure S11b-c). It is therefore rational to consider an alloying effect with Ni as a great contribution to the activity improvement of our PdNi HNS aerogels. In addition, the hollow architecture of the building blocks accompanied by the aerogel nature confers high porosity and large surface area on the HNS aerogel which facilitate mass transfer and endue more active sites for catalysis. The synergy of the aforementioned effects constitute jointly the large activity improvement of the PdNi HNS aerogels, while the self-supportability ensures great potential in the durability due to the escape from the general carbon corrosion.[7] As shown in Figure 3d, chronoamperometry was employed to evaluate the stabilities of the HNS aerogel catalyst with the Pd83Ni17 HNS aerogel exhibiting a much higher initial polarization current densities and slower current decays than the Pd/C, demonstrating the promising industrial prospect of the as-prepared HNS aerogel electrocatalysts.

In summary, we have reported on a function-led design of metallic aerogels, inside which the alloyed PdNi HNS building blocks connect and fuse into a well-defined 3D network. The aerogel nature and the hollow building blocks confer several advantages such as high porosity, large surface area, efficient electron transfer routes and self-supportability upon the PdNi HNS aerogels. These properties, accompanied with the Ni doping, qualify the PdNi HNS aerogels to be promising electrocatalysts towards the oxidation of ethanol. The morphology and shell thickness of the building blocks are strongly dependent on their composition which can be tuned by controlling of the Ni/Pd precursor ratios. Among them, the Pd83Ni17 HNS aerogel exhibits the highest MA and SA that are 5.6- and 4.2-fold higher than those of the commercial Pd/C. The work highlights the great potential of metallic aerogels as highly efficient electrocatalysts through morphology and composition control of the building blocks and could be further generalized for many other electrochemical reactions by the utilization of appropriate metals.

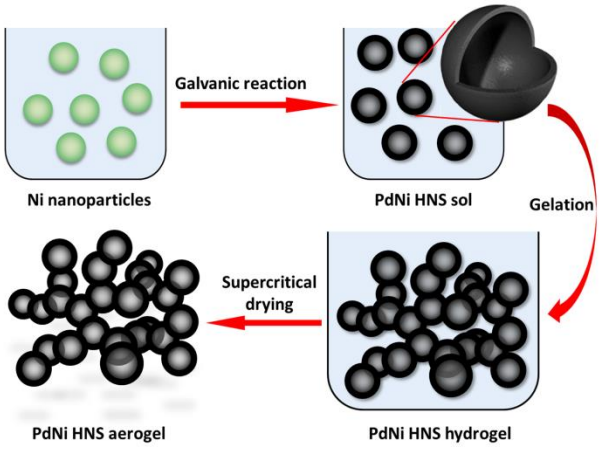

Scheme 1. Illustration of the synthesis procedure.

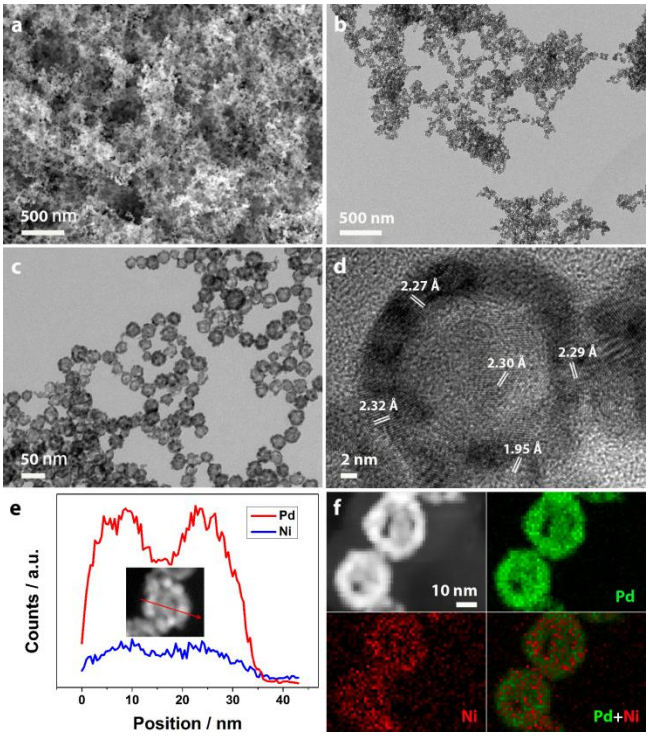

Figure 1. a) SEM and b,c) TEM images of the $Pd_{83}Ni_{17}$ HNS aerogel at different magnifications. d) HR-TEM characterization of the fused connection and an HNS area only of the $Pd_{83}Ni_{17}$ HNS aerogel. STEM-EDX e) line-scanning profiling and f) high angle annular dark field (HAADF) STEM imaging and elemental mapping analysis of Pd and Ni.

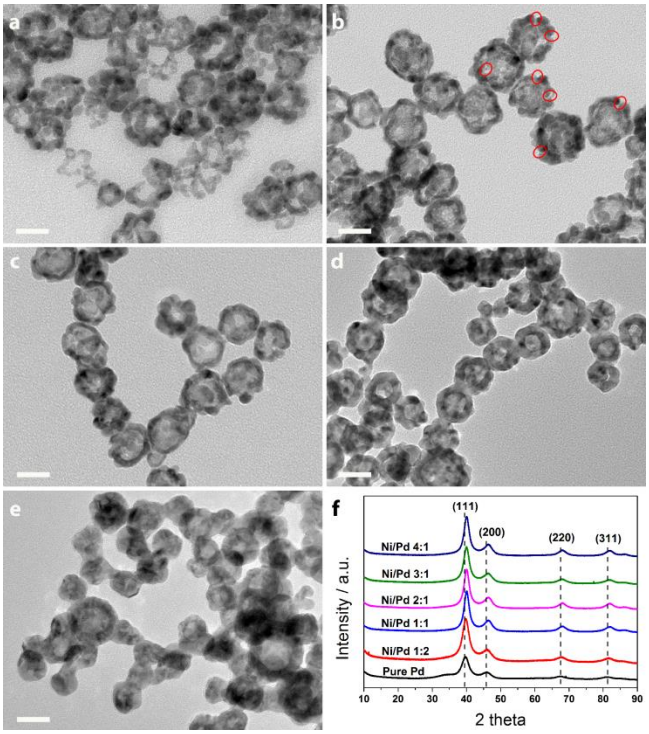

Figure 2. TEM images of Pd_xNi_y HNS aerogels with different Ni/Pd precursor ratios: a) 4:1, b) 3:1, c) 2:1, d) 1:1 and e) 1:2. Scale bar is 20 nm. f) XRD analysis of Pd_xNi_y HNS aerogels with different Ni/Pd precursor ratios.

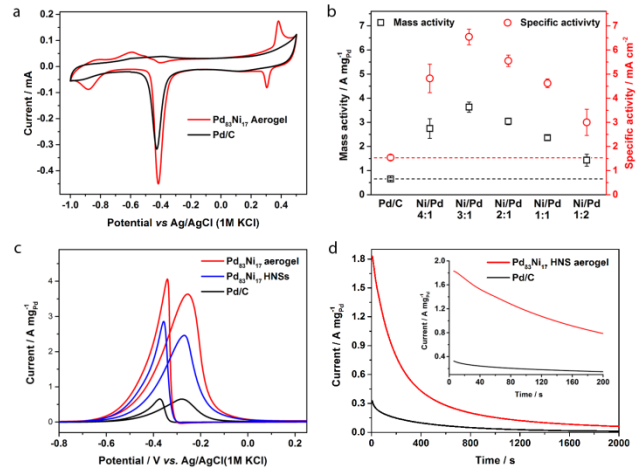

Figure 3. a) Comparison of the CVs of the $Pd_{83}Ni_{17}$ HNS aerogel and a commercial Pd/C in N_2-saturated 1 M NaOH solution. Loading of Pd is 20 μg cm^{-2}. Scan rate: 100 mV s^{-1}. b) The mass and specific activities of PdNi HNS aerogels with different Ni/Pd precursor ratios and commercial Pd/C. c) Pd mass normalized CVs of the $Pd_{83}Ni_{17}$ HNS aerogel and the $Pd_{83}Ni_{17}$ HNSs in N_2-saturated 1 M NaOH + 1 M ethanol solution. Scan rate: 50 mV s^{-1}. d) The Pd mass normalized i-t curves of the $Pd_{83}Ni_{17}$ HNS aerogel and commercial Pd/C in N_2-saturated 1 M NaOH + 1 M ethanol solution.

References

[1] Ren, W. C.; Cheng, H. M., *Nature* **2013**, *497*, 448.

[2] a) Kistler, S. S., *Nature* **1931**, *127*, 741; b) Hüsing, N.; Schubert, U., *Angew. Chem.* **1998**, *110*, 22; *Angew. Chem. Int. Ed.* **1998**, *37*, 22.

[3] a) Leventis, N.; Chandrasekaran, N.; Sadekar, A. G.; Sotiriou-Leventis, C.; Lu, H., *J. Am. Chem. Soc.* **2009**, *131*, 4576; b) Mahadik-Khanolkar, S.; Donthula, S.; Bang, A.; Wisner, C.; Sotiriou-Leventis, C.; Leventis, N., *Chem. Mater*. **2014**, *26*, 1318.

[4] a) Mohanan, J. L.; Arachchige, I. U.; Brock, S. L., *Science* **2005**, *307*, 397; b) Hitihami-Mudiyanselage, A.; Senevirathne, K.; Brock, S. L., *ACS Nano* **2013**, *7*, 1163.

[5] a) Gao, X.; Esteves, R. J.; Luong, T. T.; Jaini, R.; Arachchige, I. U., *J. Am. Chem. Soc.* **2014**, *136*, 7993; b) Ranmohotti, K. G. S.; Gao, X. N.; Arachchige, I. U., Chem. Mater. **2013**, *25*, 3528.

[6] a) Gaponik, N.; Wolf, A.; Marx, R.; Lesnyak, V.; Schilling, K.; Eychmüller, A., *Adv. Mater.* **2008**, 20, 4257; b) Bigall, N. C.; Herrmann, A. K.; Vogel, M.; Rose, M.; Simon, P.; Carrillo-Cabrera, W.; Dorfs, D.; Kaskel, S.; Gaponik, N.; Eychmüller, A., *Angew. Chem.* **2009**, *121*, 9911; *Angew. Chem. Int. Ed.* **2009**, *48*, 9731; c) Lesnyak, V.; Wolf, A.; Dubavik, A.; Borchardt, L.; Voitekhovich, S. V.; Gaponik, N.; Kaskel, S.; Eychmüller, A., *J. Am. Chem. Soc.* **2011**, *133*, 13413; d) Yuan, J.; Wen, D.; Gaponik, N.; Eychmüller, A., *Angew. Chem.* **2013**, *125*, 1010; *Angew. Chem. Int. Ed.* **2013**, *52*, 976.

[7] Liu, W.; Herrmann, A. K.; Bigall, N. C.; Rodriguez, P.; Wen, D.; Oezaslan, M.; Schmidt, T. J.; Gaponik, N.; Eychmüller, A., *Acc. Chem. Res.* **2015**, *48*, 154.

[8] Gaponik, N.; Herrmann, A.-K.; Eychmüller, A., *J. Phys. Chem. Lett.* **2011**, *3*, 8.

[9] a) Liu, W.; Rodriguez, P.; Borchardt, L.; Foelske, A.; Yuan, J.; Herrmann, A. K.; Geiger, D.; Zheng, Z.; Kaskel, S.; Gaponik, N.; Kotz, R.; Schmidt, T. J.; Eychmüller, A., *Angew. Chem.* **2013**, *125*, 10033; *Angew. Chem. Int. Ed.* **2013**, *52*, 9849; b) Wen, D.; Herrmann, A. K.; Borchardt, L.; Simon, F.; Liu, W.; Kaskel, S.; Eychmüller, A., *J. Am. Chem. Soc.* **2014**, *136*, 2727.

[10] Wang, Y. J.; Zhao, N.; Fang, B.; Li, H.; Bi, X. T.; Wang, H., *Chem. Rev.* **2015**, *115*, 3433.

[11] a) Xia, X.; Wang, Y.; Ruditskiy, A.; Xia, Y., *Adv. Mater*. **2013**, *25*, 6313; b) Stamenkovic, V. R.; Fowler, B.; Mun, B. S.; Wang, G.; Ross, P. N.; Lucas, C. A.; Markovic, N. M., *Science* **2007**, *315*, 493.

[12] Baldizzone, C.; Mezzavilla, S.; Carvalho, H. W.; Meier, J. C.; Schuppert, A. K.; Heggen, M.; Galeano, C.; Grunwaldt, J. D.; Schuth, F.; Mayrhofer, K. J., *Angew. Chem.* **2014**, *126*, 14474; *Angew. Chem. Int. Ed.* **2014**, *53*, 14250.

[13] Liu, W.; Herrmann, A. K.; Geiger, D.; Borchardt, L.; Simon, F.; Kaskel, S.; Gaponik, N.; Eychmüller, A., *Angew. Chem.* **2012**, *124*, 5841; *Angew. Chem. Int. Ed.* **2012**, *51*, 5743.

[14] Guo, S.; Zhang, S.; Sun, S., *Angew. Chem.* **2013**, *125*, 8686; *Angew. Chem. Int. Ed*. **2013**, *52*, 8526.

[15] Xia, B. Y.; Wu, H. B.; Li, N.; Yan, Y.; Lou, X. W.; Wang, X., *Angew. Chem.* **2015**, *127*, 3868; *Angew. Chem. Int. Ed.* **2015**, *54*, 3797.

[16] Xiao, L.; Zhuang, L.; Liu, Y.; Lu, J.; Abruna, H. D., *J. Am. Chem. Soc.* **2009**, *131*, 602.

[17] Zhao, X.; Chen, S.; Fang, Z.; Ding, J.; Sang, W.; Wang, Y.; Zhao, J.; Peng, Z.; Zeng, J., *J. Am. Chem. Soc.* **2015**, *137*, 2804.